

THE QCD PHASE DIAGRAM AT HIGH DENSITIES: AN EXPERIMENTAL OVERVIEW*

CHRISTOPH BLUME

Institut für Kernphysik, Goethe-Universität Frankfurt
Max-von-Laue-Str. 1, 60438 Frankfurt, Germany

*Received 29 January 2024, accepted 11 March 2024,
published online 23 April 2024*

In this contribution, we review on-going and planned experimental programs addressing the study of the QCD phase diagram at high net-baryon densities. Several physics observables relevant for these investigations are discussed. Special emphasis is put on physics topics of interest in the energy region accessible at FAIR, currently under construction in Darmstadt, Germany.

DOI:10.5506/APhysPolB.55.5-A3

1. Introduction

1.1. The QCD phase diagram

The study of the QCD phase diagram is one of the main topics of heavy-ion physics and is being addressed by several on-going and planned experimental programs. Currently, there are only very limited experimental facts available on the features of the phase diagram, which are summarized in Fig. 1, together with several theoretical predictions. While for vanishing μ_B , *i.e.* measurements at LHC or top-RHIC energies, lattice QCD calculations agree on the presence of a crossover (yellow band) between a hadron gas and a Quark–Gluon Plasma (QGP), at higher μ_B , a first-order phase boundary is expected, which should end in a critical endpoint. However, in this region, theoretical predictions are still very difficult since lattice-QCD methods become unreliable beyond $\mu_B/T > 2-3$ and effective models have to be used. This is evident from the different results compiled in Fig. 1 which have been derived with functional renormalisation group (fRG) and Dyson–Schwinger-equation calculations. The only real experimental input currently available in this region are the chemical freeze-out points, extracted from statistical model analyses of measured particle yields, which are also included in Fig. 1.

* Presented at the LXIII Cracow School of Theoretical Physics *Nuclear Matter at Extreme Densities and High Temperatures*, Zakopane, Poland, 17–23 September, 2023.

For instance, an unambiguous evidence in experimental data for the presence of a first-order phase boundary is still lacking and this presents, therefore, an important task to be addressed in the future. This is also a prerequisite for the ultimate goal of identifying the existence and location of the critical endpoint with measured data.

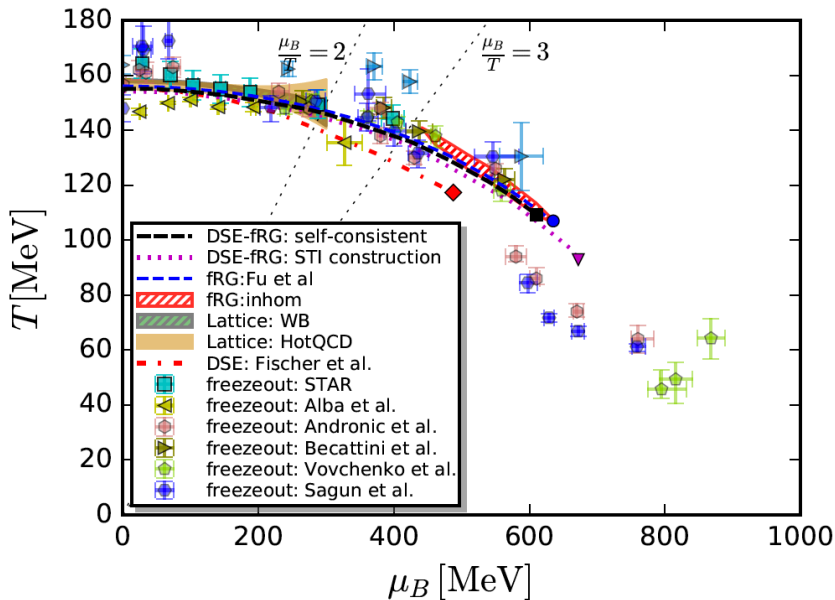


Fig. 1. The QCD phase diagram including calculations of the deconfinement crossover line following from different theoretical approaches, such as functional renormalisation group (fRG), Dyson–Schwinger equation (DSE), and lattice QCD, together with corresponding predictions of the critical endpoint [1]. Also shown are chemical freeze-out points extracted from data using different statistical model approaches.

1.2. Baryon number distributions

To experimentally probe the different regions of the QCD phase diagram, one has to prepare the reaction systems in a way that they will follow different trajectories in the T – μ_B plane. The main experimental control variable for this purpose is the center-of-mass energy of the colliding nuclei, $\sqrt{s_{NN}}$. Figure 2 schematically illustrates how the baryon number, initially contained in the projectile and target nucleus before the collision, is distributed after the collision has taken place at lower energies (*e.g.* AGS, RHIC-BES or FAIR, left panel) and at higher energies (*e.g.* RHIC and LHC, right panel). The average rapidity shift $\langle\delta y\rangle$, experienced by the baryons, grows less than linearly with the projectile rapidity y_P , *i.e.* $\langle\delta y\rangle/y_P$ drops with increasing

Lower energies:

Higher energies:

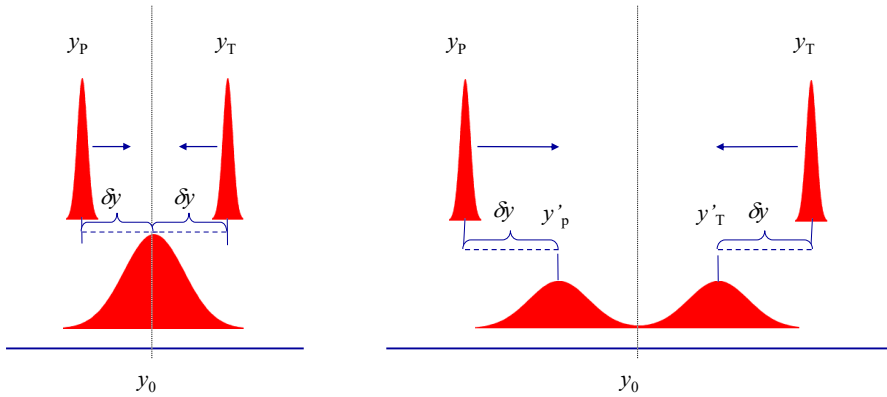


Fig. 2. Schematic depiction of the projectile and target baryon number rapidity distributions before ($y_{P,T}$, upper pictures) and after ($y'_{P,T}$, lower pictures) a heavy-ion collision. Shown is the scenario at lower energies (left panel) and higher energies (right panel), together with the corresponding rapidity shift ($\delta y = y_{P,T} - y'_{P,T}$). Mid-rapidity is denoted by y_0 .

$\sqrt{s_{NN}}$ [2, 3]. While at low energies most of the initial baryons will, therefore, be shifted to the region around mid-rapidity, y_0 , at high energies, less and less of them will end up there and, consequently, the net-baryon number around y_0 will decrease with increasing $\sqrt{s_{NN}}$. This is directly reflected in the energy dependence of the antibaryon–baryon ratios, as depicted in the left panel of Fig. 3. These ratios approach unity at high $\sqrt{s_{NN}}$ since

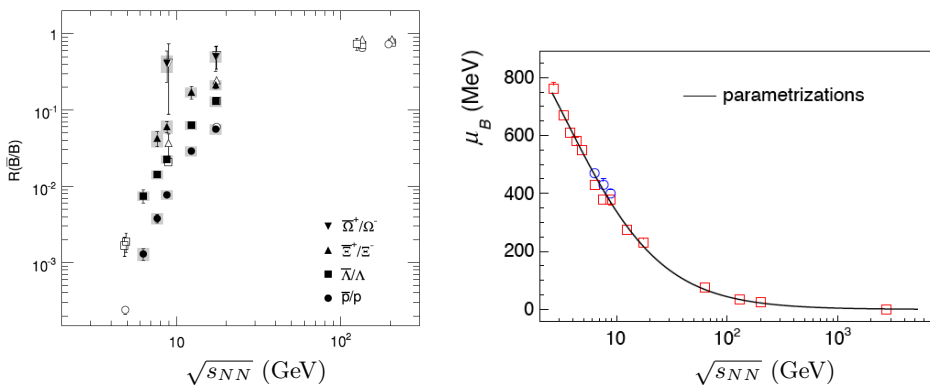


Fig. 3. Left: the antibaryon–baryon ratios measured around mid-rapidity in central Pb+Pb and Au+Au collisions as a function of $\sqrt{s_{NN}}$ [4]. Right: the baryo-chemical potential μ_B as extracted from statistical model fits to data at different $\sqrt{s_{NN}}$ [5]. Shown is also the parametrization μ_B [MeV] = $1307.5 / (1 + 0.288 \times \sqrt{s_{NN}} [\text{GeV}])$ as a solid black line.

the net-baryon density in the fireball region vanishes at high energies. As the baryo-chemical potential μ_B is directly dependent on these ratios, *e.g.* as $n_{\bar{p}}/n_p = \exp(-2\mu_B/T)$ in the case of the antiproton–proton ratio, μ_B decreases monotonically with $\sqrt{s_{NN}}$ (see the right panel of Fig. 3). Using parametrizations, such as the one represented by the solid line, one can easily translate a given $\sqrt{s_{NN}}$ into the value of μ_B to be expected for this reaction system, at least for central collisions.

1.3. Relation to neutron star mergers

Heavy-ion collisions at lower energies, dominated by high net-baryon densities, can create nuclear matter with properties very similar to those in the central region of binary neutron star (BNS) mergers. Such astrophysical events have been observed via the emitted gravitational waves [6] and are also discussed in detail in [7]. Figure 4 shows a comparison between a simulation of a BNS merger event (upper row) and a non-central heavy-ion collision at $\sqrt{s_{NN}} = 2.42$ GeV (lower row), as studied by the HADES experiment.

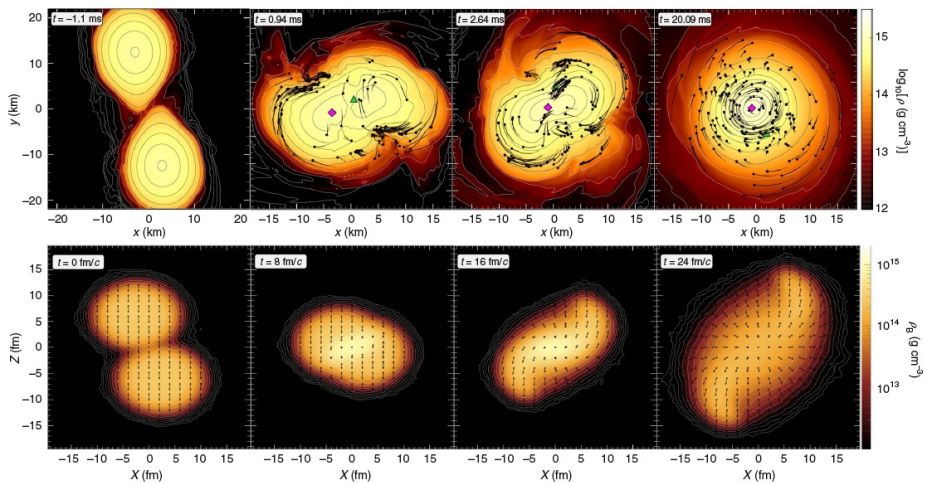


Fig. 4. Top row: simulation of a binary neutron star merger for two neutron stars with equal masses of $1.35 M_{\odot}$. The densities reach five times the saturation density and the temperatures approach values close to 20 MeV. Bottom row: simulation of the time evolution of the energy density achieved in a non-central heavy-ion collision at $\sqrt{s_{NN}} = 2.42$ GeV. Densities reach up to three times normal matter density and temperatures up to 80 MeV. While densities and temperatures are similar, the scales for space and time are naturally different: kilometer for the neutron star merger and femtometer in the case of the heavy-ion collision. Likewise, the durations of the collision events differ by 20 orders of magnitude [8].

It is found that densities and temperatures reached in both cases are very similar. In addition to the exploration of the QCD phase diagram, heavy-ion collisions are, therefore, also an important instrument for the study of neutron star matter in the laboratory.

2. Experiments at high μ_B

2.1. Experiments overview

Experimental heavy-ion physics has a history dating back to the early eighties, where first pioneering experiments (Plastic Ball, Streamer Chamber) were performed at the Bevalac (LBNL, Berkeley). Since then, the interest moved on to higher beam energies, like the ones available at the AGS at BNL and the SPS at CERN. The high-energy frontier was moved up further once RHIC started operating in the year 2000 and ultimately reached the highest collision energies currently available at the LHC in 2009. While the experiments at the high-energy and low- μ_B frontier delivered many exciting results on the QGP properties, and continue to do so, in the meantime, a strong interest has also developed in the systematic exploration of the high- μ_B region. Previous experiments at the SIS18, AGS, and SPS have already provided many important measurements in the relevant energy regime in the past. However, due to limitations in the detector technology and the achievable collision rates, most available data sets are restricted to more abundant bulk particles (*e.g.* p , π , K , Λ , ...) and have relatively large uncertainties. In order to make substantial progress in this area, new generation experiments are needed that can digest high-interaction rates, so that sufficient statistics for systematic and multi-differential studies can be reached and also rare probes can be investigated with high precision.

Figure 5 summarizes existing and planned heavy-ion experiments. Shown is the achieved or projected interaction rate *versus* the center-of-mass energy range studied by a given experiment. Currently running experiments are mostly operating at interaction rates of the order of 10^3 Hz, with the exception of HADES and the upgraded ALICE setup reaching $> 10^4$ Hz. Planned facilities, in particular those at low energies, aim at substantially higher values. This includes the NA60+ experiment at the CERN-SPS (2×10^5 Hz), CEE at HIAF in Lanzhou, China (5×10^5 Hz), the heavy-ion facility at J-PARC in Tokai, Japan (10^7 Hz), and CBM at FAIR in Darmstadt, Germany (10^7 Hz).

From Fig. 5 it is obvious that high-interaction rates are much easier achieved in fixed target setups, provided the accelerator is able to deliver high-beam intensities. This is much more difficult in collider configurations, as high-beam luminosities require very precise beam focussing. This is in

particular problematic when the collision energies are lowered, as is evident from the blue stars in Fig. 5, which represent the interaction rates seen by STAR at RHIC for different energies.

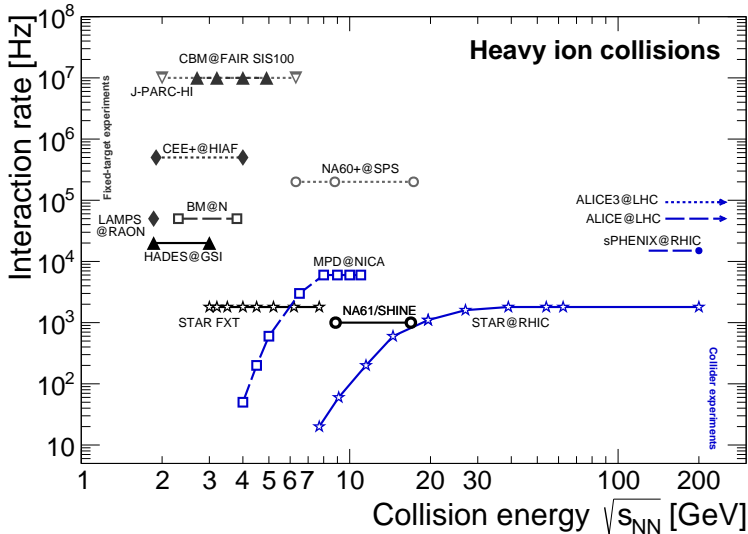


Fig. 5. The interaction rates achieved by existing and planned heavy-ion facilities as a function of $\sqrt{s_{NN}}$. Blue symbols denote experiments in collider mode, while black and grey symbols represent those in fixed-target mode. Solid curves correspond to running facilities, respectively experiments, long-dashed curves to approved ones, and short-dashed curves to those in the conceptual design stage [9].

On the other hand, collider experiments have the advantage that the detector acceptance is independent of the collision energy, which facilitates the comparison of results for different $\sqrt{s_{NN}}$. This is not as straight-forward for fixed-target experiments where the acceptance can vary significantly at different beam energies. To a certain extent, this can be mitigated by scaling the magnetic field in the spectrometer accordingly.

2.2. The STAR beam energy scan program

A wealth of data on the high- μ_B region of the phase diagram has been collected in recent years in the context of the Beam Energy Scan (BES) program of the STAR Collaboration at RHIC. The experimental setup of STAR has recently been upgraded by an event plane detector, an endcap TOF, and new inner readout chambers for the TPC (see the top panel of Fig. 6). This allowed the collaboration to take data over a very wide range of $\sqrt{s_{NN}}$ (see the bottom panel of Fig. 6). For data taking in the very low-

energy region ($\sqrt{s_{NN}} < 7.7$ GeV), the FiXeD Target (FXT) configuration is exploited, in which an internal target is placed into the beam pipe at the entrance of the TPC. A selection of results from the STAR-BES program can be found in [10–13].

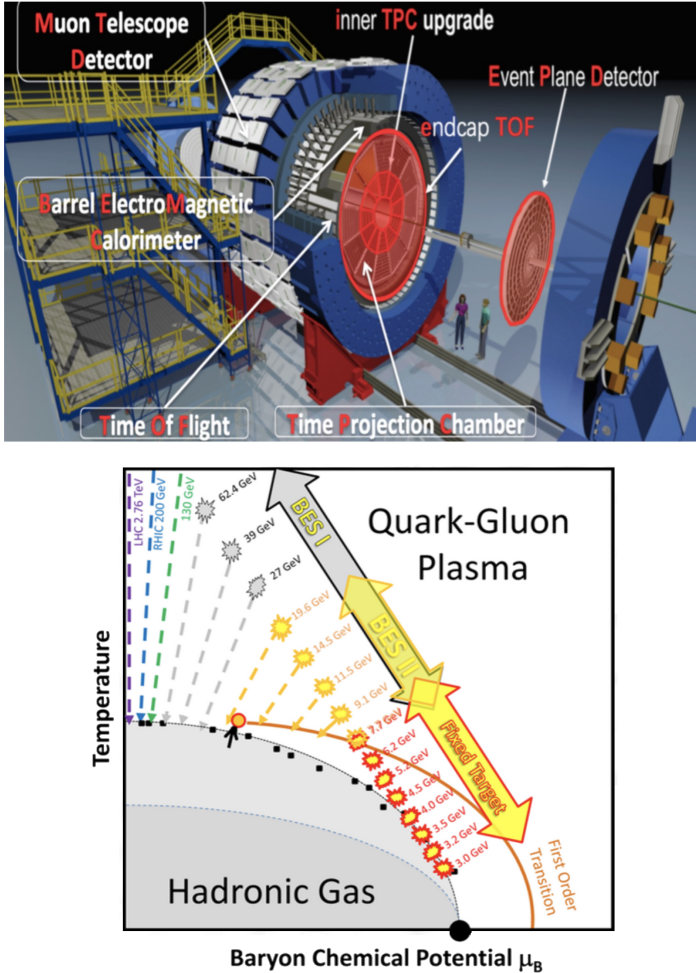


Fig. 6. Top: picture of the upgraded STAR experiment. Bottom: the different center-of-mass energies studied during the beam energy scan periods (BES-I and BES-II) and the fixed target campaign (FXT) [14].

2.3. Experiments at GSI/FAIR: HADES and CBM

The HADES experiment is currently performing an extensive program including heavy-ion collisions at different beam energies and reactions of

proton and pion beams with proton and nuclear targets at the SIS18 accelerator of GSI in Darmstadt, Germany. The upgraded experimental setup is shown in the top panel of Fig. 7. Due to the full stopping, heavy-ion reactions at these energies ($\sqrt{s_{NN}} = 2.42$ GeV for Au+Au, $\sqrt{s_{NN}} = 2.55$ GeV for Ag+Ag) are dominated by baryons (with $\sim 50\%$ of the nucleons bound in light clusters) and, therefore, cover the region of highest baryo-chemical potential ($\mu_B \approx 750\text{--}800$ MeV, see the bottom panel of Fig. 7).

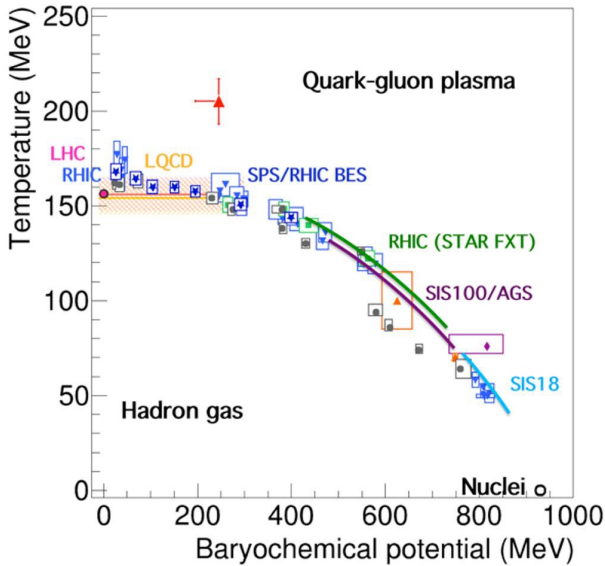
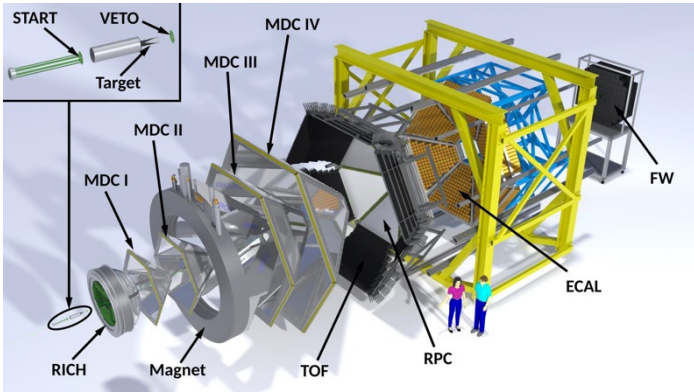


Fig. 7. Top: picture of the current HADES setup. Bottom: location of the chemical freeze-out point in the $T\text{--}\mu_B$ plane as extracted from Au+Au data measured with HADES at $\sqrt{s_{NN}} = 2.42$ GeV [15].

The construction of the FAIR accelerator complex is currently approaching its completion and CBM, the dedicated heavy-ion experiment at this facility, is being constructed. It will allow to investigate the high- μ_B region of the phase diagram with unprecedented precision as it is being designed to operate at peak interaction rates of 10^7 Hz. Figure 8 presents the experimental setup of CBM, which is discussed in detail in this contribution [16]. A review of the CBM physics program can be found here [17].

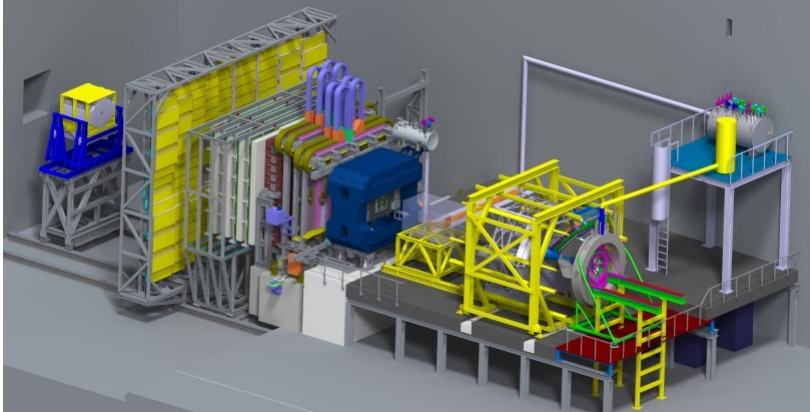


Fig. 8. Drawing of the planned setup of the CBM experiment [16]. Also shown is the HADES experiment on the right, which is supposed to be transferred to the CBM cave after the completion of its physics program at the SIS18.

2.4. Experiments at the CERN-SPS: NA61 and NA60+

The SPS at CERN has a long, dating back to the eighties, history of many different fixed target heavy-ion experiments which is still on-going strongly. Currently, the NA61/SHINE experiment is completing its physics program of a two-dimensional scan which varies the beam energy as well as the system size (see the bottom panel of Fig. 9). The experimental setup, shown in the top panel of Fig. 9, is based on upgraded detectors of the NA49 experiment which have been complemented with several new components.

Another proposed experiment that is currently under consideration is a modern version of the previous NA60 experiment, called NA60+ at the moment. This is foreseen as a dimuon spectrometer for high-beam intensities (see the top panel of Fig. 10). The project aims at a systematic study of J/ψ production, to locate the onset of J/ψ suppression, open charm production and of intermediate-mass dileptons in the $\sqrt{s_{NN}}$ interval between ~ 6 –17 GeV. The latter will allow to determine the $\sqrt{s_{NN}}$ evolution of the

effective early-stage temperature of the fireball in an energy region complementary to the CBM program (see the bottom panel of Fig. 10). For a detailed discussion, see Section 3.4.

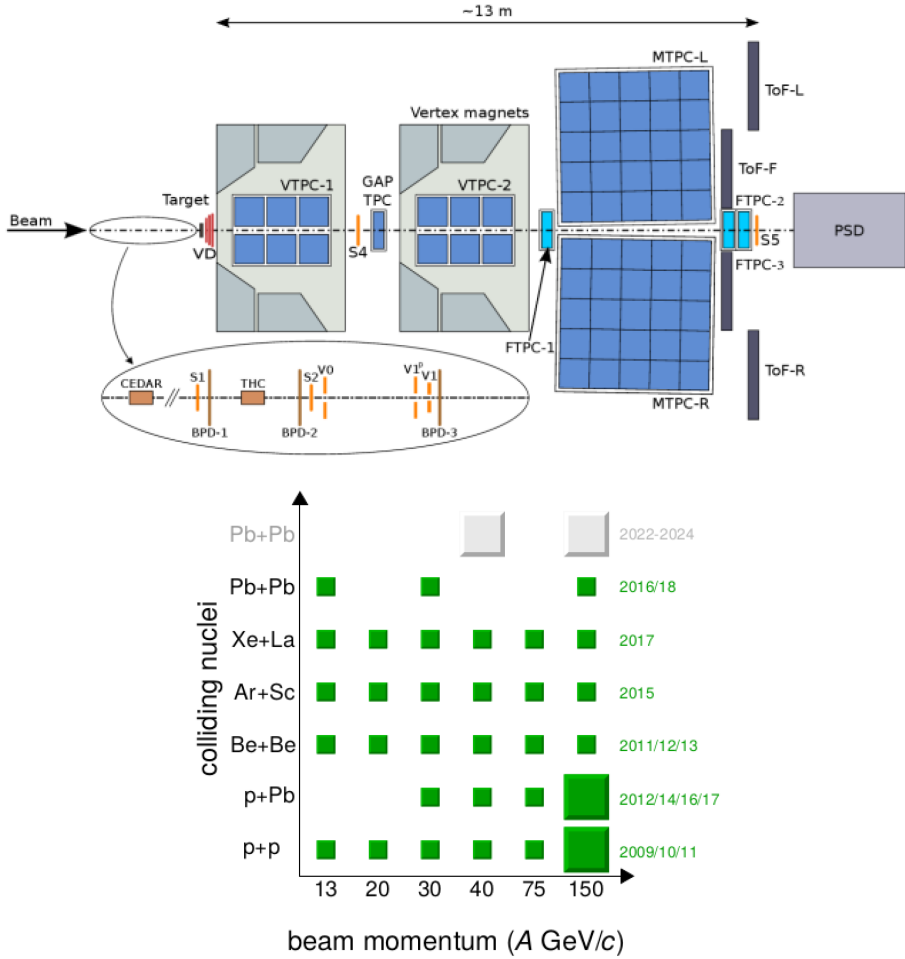


Fig. 9. Top: schematic drawing of the setup of the NA61/SHINE experiment. Bottom: the data samples collected by NA61/SHINE for different collision systems and beam energies [18].

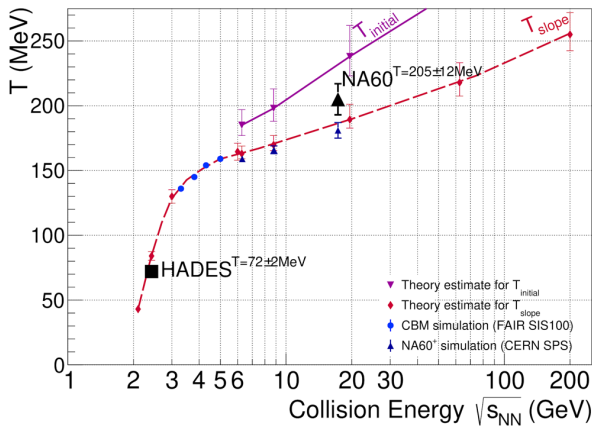
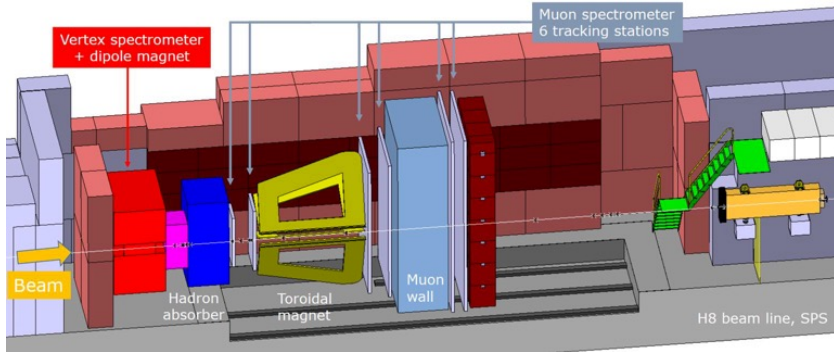


Fig. 10. Top: drawing of the projected NA60+ experiment. Bottom: expected performance for the extraction of the effective fireball temperature from intermediate-mass dileptons for NA60+ and CBM (blue symbols) as a function of $\sqrt{s_{NN}}$ [19].

3. Observables

In the following, we will discuss several observables of high relevance for the understanding of the QCD phase diagram at high μ_B . This list is of course a personal selection and many other interesting topics are omitted for the sake of length. One very important observable not addressed here is the measurement of fluctuations of conserved charges, as this is discussed in detail in [20].

3.1. Collectivity

Collective effects are one of the earliest observables studied in heavy-ion physics and their investigation has yielded a multitude of information on the properties of nuclear matter under extreme conditions [21–24].

Pressure is generated throughout the whole evolution of the fireball created in heavy-ion collisions, both in the hadronic and, at higher energies, also in the partonic phase. This pressure modifies the particle spectra and thus provides information on the matter properties, such as its equation-of-state (EOS), affected by the degrees of freedom of the medium constituents, and its viscosity. The transverse mass spectra experience a blue shift, due to the radial expansion velocity β_T of the system, *i.e.* their inverse slope parameter as extracted with a Boltzmann fit will exhibit higher values. A more refined method of simultaneously determining the kinetic freeze-out temperature T_{kin} and the average transverse expansion velocity $\langle\beta_T\rangle$ of the fireball is the use of the blast wave model [25]. Figure 11 presents a summary by the STAR Collaboration of the radial flow parameters T_{kin} and $\langle\beta_T\rangle$ as a function of $\sqrt{s_{NN}}$, together with the chemical freeze-out temperature T_{ch} [10]. The kinetic freeze-out temperature T_{kin} rises rapidly for lower energies ($\sqrt{s_{NN}} \lesssim 7$ GeV) and then seems to saturate or even drop. Similarly, $\langle\beta_T\rangle$ rises quickly at low energies and then experiences only a moderate further increase above roughly the same energy. This might be indicative of the onset of new, partonic degrees of freedom which soften the EOS.

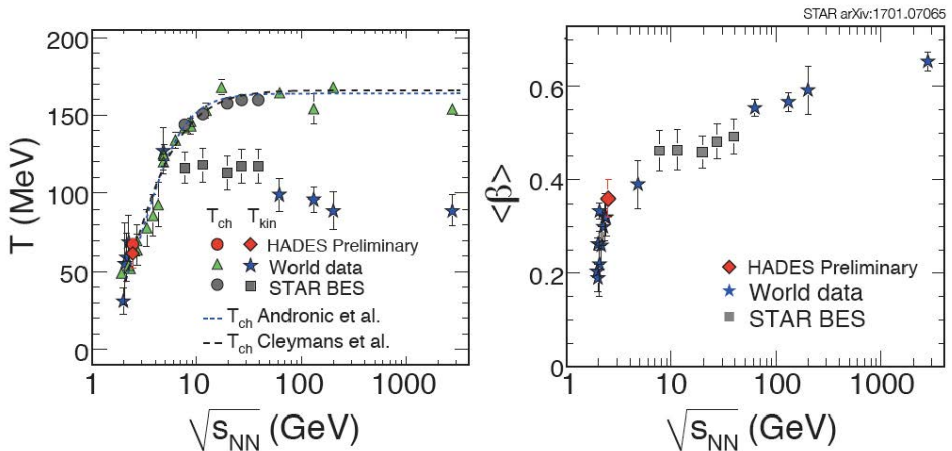


Fig. 11. Left: the kinetic freeze-out temperature (T_{kin}), as extracted with fits of the blast-wave model to transverse momentum spectra, and the chemical freeze-out temperature (T_{ch}) determined with statistical model fits, both as a function of $\sqrt{s_{NN}}$. Right: the average expansion velocity $\langle\beta_T\rangle$ from blast-wave-model fits as a function of $\sqrt{s_{NN}}$ [10].

Beyond the radial flow, also higher moments of the particle emission pattern relative to the reaction plane can be extracted. As the reaction plane, defined by the beam axis and the direction of the impact parameter vector, cannot be measured directly, one relies on the so-called event plane which

can, *e.g.*, be determined from the event-by-event azimuthal distribution of the spectator nucleons and which is correlated to the reaction plane with a given dispersion¹. Non-isotropies in the distribution of particle emission in azimuth angle ϕ relative to the event plane orientation Ψ_{EP} are quantified via a Fourier decomposition

$$E \frac{d^3N}{dp^3} = \frac{d^2N}{\pi dy d(p_t^2)} \left[1 + 2 \sum_{n=1}^{\infty} v_n(p_t, y) \cos n(\phi - \Psi_{EP}) \right]. \quad (1)$$

The first moment, v_1 , is called directed flow, while the second order, v_2 , is called elliptic flow. Higher moments can also be extracted, if the available statistics is high enough [26]. Figure 12 presents a summary of the $\sqrt{s_{NN}}$ dependence of the directed (left panel) and elliptic (right panel) flow for protons. The directed flow, quantified by the slope of v_1 around mid-rapidity, is characterized by a distinct maximum at low energies ($\sqrt{s_{NN}} \approx 2$ GeV), caused by the bounce-off effect of the spectators, which drops to zero around $\sqrt{s_{NN}} \approx 10$ GeV and then stays slightly negative.

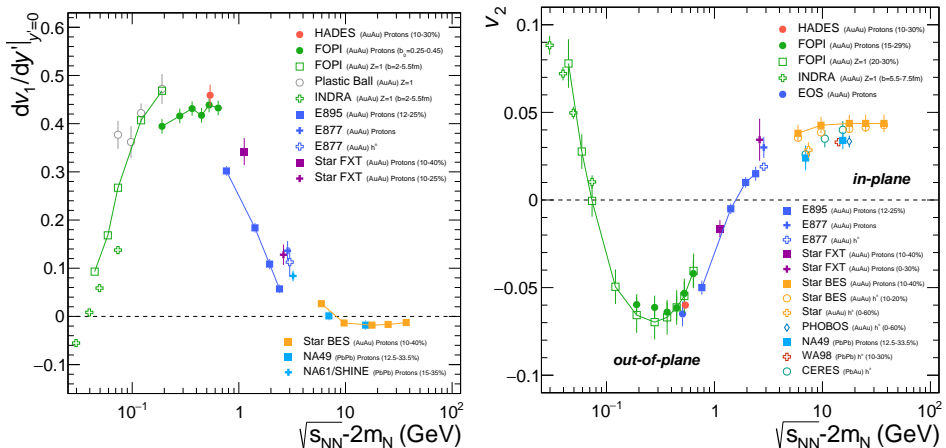


Fig. 12. Compilation of directed and elliptic flow measurements for protons as a function of the subtracted centre-of-mass energy $\sqrt{s_{NN}} - 2m_N$ (m_N : nucleon mass). Shown is the slope of v_1 at mid-rapidity $dv_1/dy'|_{y'=0}$ (left) and the p_t integrated v_2 at mid-rapidity (right) [27].

The elliptic flow has a similarly complex energy dependence. While being positive at very low energies, it turns negative around $\sqrt{s_{NN}} \approx 1.9$ GeV, *i.e.* particle emission is out-of-plane. After passing through a minimum,

¹ Please note that at higher energies, the flow coefficients are mainly extracted via the cumulant method which does not rely on an event-plane determination and also allows to suppress non-flow contributions to the measured v_n .

v_2 crosses zero around $\sqrt{s_{NN}} \approx 3.5$ GeV and slowly increases further, corresponding to the in-plane emission. While the out-of-plane emission is caused by the squeeze-out effect due to the presence of the passing spectators, the in-plane emission at higher energies is entirely the result of the higher pressure gradient in the fireball in the reaction plane compared to the direction perpendicular to it.

High-precision data on the different flow coefficients should help to limit the possible values of the viscosity of the baryonic medium, which up-to-now was much more difficult to determine than at higher energies where it is characterized by partonic degrees of freedom. Also, such data are essential for narrowing down the possible EOS of super-dense matter, which is highly relevant for the understanding of high-mass neutron stars (*i.e.* $M_{NS} \approx 2 M_{\odot}$) [28].

3.2. Vorticity

Non-central heavy-ion collisions create systems characterized by very large total angular momenta ($|L| \sim 10^5 \hbar$), which allows to create matter with extremely high vorticities ($\omega \approx 10^{21} \text{ s}^{-1}$) [29]. The total angular momentum of the medium will, under certain conditions, translate into a global polarization of particle emission. This can most easily be measured for the Λ hyperon, as the proton resulting from its decay ($\Lambda \rightarrow p + \pi^-$) will be preferentially emitted into the spin direction of the Λ . Using the relation

$$P_{\Lambda} = \frac{8}{\pi \alpha_{\Lambda}} \frac{\Psi_{\text{EP}} - \psi_p^*}{R_{\text{EP}}}, \quad (2)$$

with the Λ decay parameter α_{Λ} , the event plane angle Ψ_{EP} , the proton azimuthal angle relative to the event plane ψ_p^* , and the event plane resolution R_{EP} , the global Λ polarization P_{Λ} can be determined [30].

Figure 13 shows a compilation of recent measurements of P_{Λ} as a function of $\sqrt{s_{NN}}$. While the polarization is compatible with zero at high energies, it rapidly rises towards lower energies, reaching its highest observed values for $\sqrt{s_{NN}} \approx 2.5$ GeV. For very low energies, P_{Λ} should vanish again, as the relative momentum between the nuclei approaches zero. However, up to now no, clear evidence for a drop has been seen. The measured values for P_{Λ} are found to be in good agreement with predictions by 3D-fluid-dynamics employing different EOS [31].

3.3. Strangeness and hypernuclei

The measurement of strange particles in the high- μ_B region will be of very high importance. In particular, multi-strange (anti-)baryons provide valuable information on the nature of the produced matter, since they are

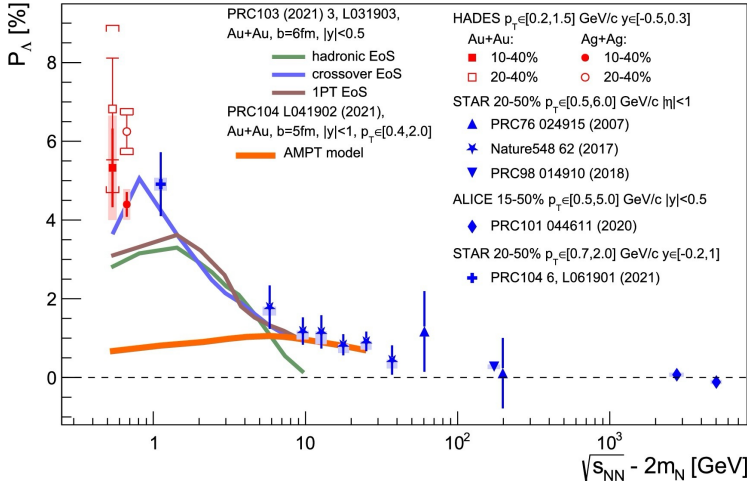


Fig. 13. Global polarization of hyperons as a function of $\sqrt{s_{NN}} - 2m_N$ (m_N : nucleon mass), measured by HADES, STAR, and ALICE [32]. Model calculations based on 3D-fluid-dynamics are shown for different EOS [31], as well as a prediction by the AMPT model [33].

extremely difficult to produce in simple hadronic interactions at these energies. The production of strange particles relative to non-strange particles is, in fact, maximal in the region of $\sqrt{s_{NN}} \approx 6-8$ GeV. This manifests itself in structures as the “horn” [34], but also in a local maximum of the Λ production rate, as shown in the upper left panel of Fig. 14. Measurements of the rare multi-strange anti-baryons ($\bar{\Xi}^+$ and $\bar{\Omega}^+$) are currently restricted to higher center-of-mass energies and data for $\sqrt{s_{NN}} < 6$ GeV would be of high relevance.

The maximum of the relative strangeness production at higher μ_B also favours the production of hypernuclei, in which one or more nucleon is replaced by a hyperon. Figure 15 shows a prediction of the yield of different hypernuclei based on a statistical model implementation [35]. Maxima are expected for $\sqrt{s_{NN}} \approx 5-7$ GeV, which will be well covered by the CBM experiment. In combination with the projected high interaction rates, FAIR will thus be an ideal facility for the precise measurement of many different hypernuclei, in particular double- Λ hypernuclei. These data will provide important input to the understanding of hyperon–nucleon and hyperon–hyperon interactions, which are essential for the solution of the so-called “hyperon-puzzle” in neutron stars [7].

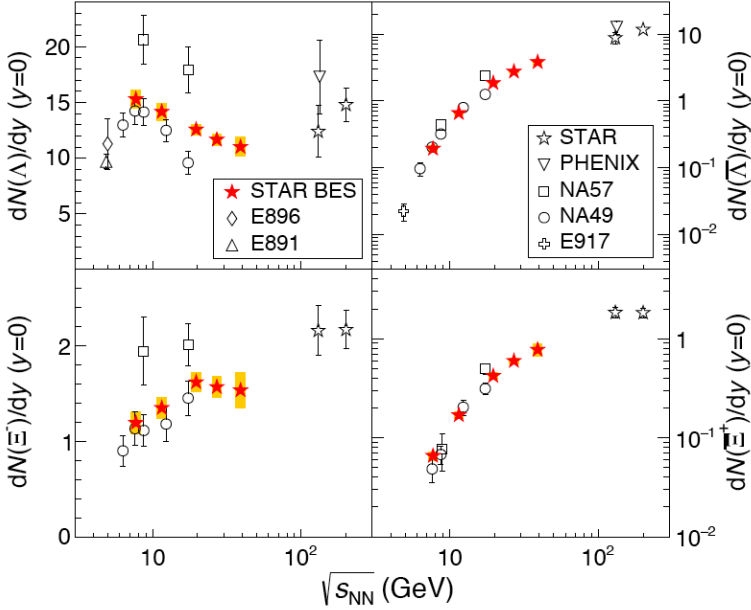


Fig. 14. The yield dN/dy at mid-rapidity of strange (anti-)baryons (Λ , $\bar{\Lambda}$, Ξ^- , $\bar{\Xi}^-$) for central Au+Au or Pb+Pb collisions as a function of $\sqrt{s_{NN}}$, as measured by experiments at the BNL-AGS (E896, E891, E917), CERN-SPS (NA49, NA57), and RHIC (STAR, PHENIX) [11].

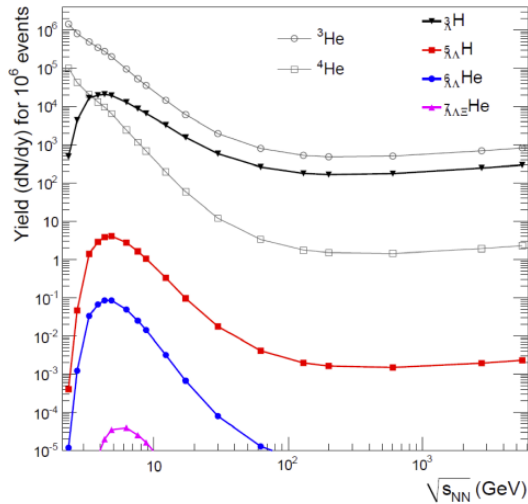


Fig. 15. Energy dependence of hypernuclei yields at mid-rapidity for 10^6 central Au+Au collisions as predicted by the statistical model [35].

Current heavy-ion experiments have already collected many new results on hypernuclei properties. The top panel of Fig. 16 shows a compilation of recent measurements of the Λ binding energy B_Λ for the hypertriton, which indicates that it is in the region of only $B_\Lambda \approx 400$ keV. This is an extremely low value² and implies that the ${}^3_\Lambda\text{H}$ wave function has a spatial extension larger than a Pb nucleus. Therefore, it is very remarkable that such fragile and huge objects can be formed in the extreme environment of a heavy-ion collision with chemical freeze-out temperatures of $T_{\text{ch}} \sim 150$ MeV, *i.e.* three orders of magnitude higher than B_Λ . This has led to the notion of the “ice in fire” or “snowball in hell” puzzle. However, recent transport model calculations are able to provide an explanation for this puzzle [36]. Here, it is found that hypernuclei are formed behind the expanding front of hot and dense hadrons where the conditions are much less severe.

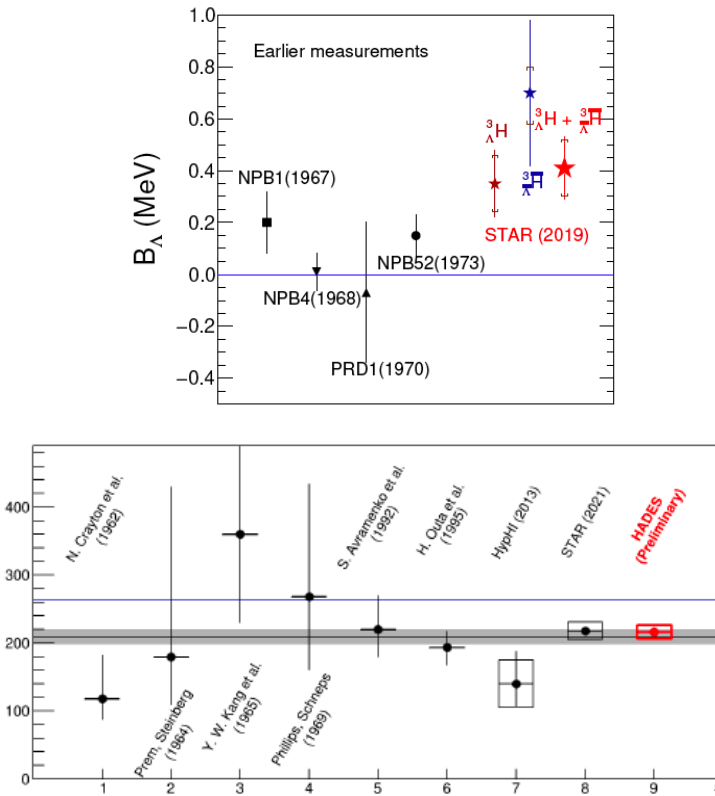


Fig. 16. Top: measurements of the Λ binding energy B_Λ in ${}^3_\Lambda\text{H}$ [37]. Bottom: recent data on the lifetime of ${}^4_\Lambda\text{H}$ [38].

² This is much lower than the deuteron binding energy $B_d = 2.2$ MeV, as an example for an already very loosely bound object.

In the recent past, some tension between different measurements of the hypertriton lifetime was found, where several experiments observed values below the one for free Λ . However, newer data rather indicate that there is no significant difference between the lifetimes [38, 39]. The situation is different for the ${}^4_\Lambda\text{H}$, where a deviation from the free Λ lifetime of 4.9σ is observed (see the bottom panel of Fig. 16).

3.4. Emissivity

Electromagnetic radiation is emitted throughout the full evolution of the fireball. As the real or virtual photons do not interact strongly, they can escape the medium unmodified and thus transport valuable information from also early stages of the fireball evolution. The main sources of virtual photons, which are reconstructed via dileptons (e^+e^- or $\mu^+\mu^-$), are in the low-mass range π^0 and η Dalitz decays and the decay of vectormesons (ρ , ω , ϕ), where the latter are sensitive to medium modifications. In the intermediate-mass range (*i.e.* below the J/ψ mass), dileptons from heavy-ion collisions in the high- μ_B region have a significant contribution from thermal radiation, as the open charm contribution is negligible, and thus convey unique information on the early-stage temperatures.

The top panel of Fig. 17 shows such a thermal component of the dilepton spectrum as measured by HADES. It has been obtained by subtracting a measured and appropriately scaled nucleon-nucleon-reference which accounts for all hadronic contributions except the ρ (*i.e.* $\pi^0/\eta \rightarrow e^+e^- \gamma$, $\omega/\phi \rightarrow e^+e^-$, $\omega \rightarrow e^+e^- \pi^0$) [8]. From this exponential spectrum of excess radiation a temperature of $T_{\text{rad}} = 71.8 \pm 2.1$ MeV can be extracted. A similar analysis has also been performed by the NA60 Collaboration for In+In collisions at $\sqrt{s_{NN}} = 17.2$ GeV [40]. The resulting temperature is shown in the bottom panel of Fig. 17 together with the HADES result as red triangles, superimposed onto the QCD phase diagram including the chemical freeze-out temperatures at different μ_B . The region between these two data points shall be populated by further high-precision measurements with CBM and NA60+ (see the bottom panel of Fig. 10) in order to establish the energy dependence of the early-stage temperatures and to search this way for any sign of a first-order phase transition.

3.5. Conclusions

There is a broad spectrum of on-going and planned experimental activities addressing the high- μ_B region of the QCD phase diagram. A lot of exciting results have been obtained in recent years by the STAR-BES and NA61/SHINE experiments. In the near future, facilities such as FAIR, J-PARC, CERN-SPS or NICA will provide unique opportunities to system-

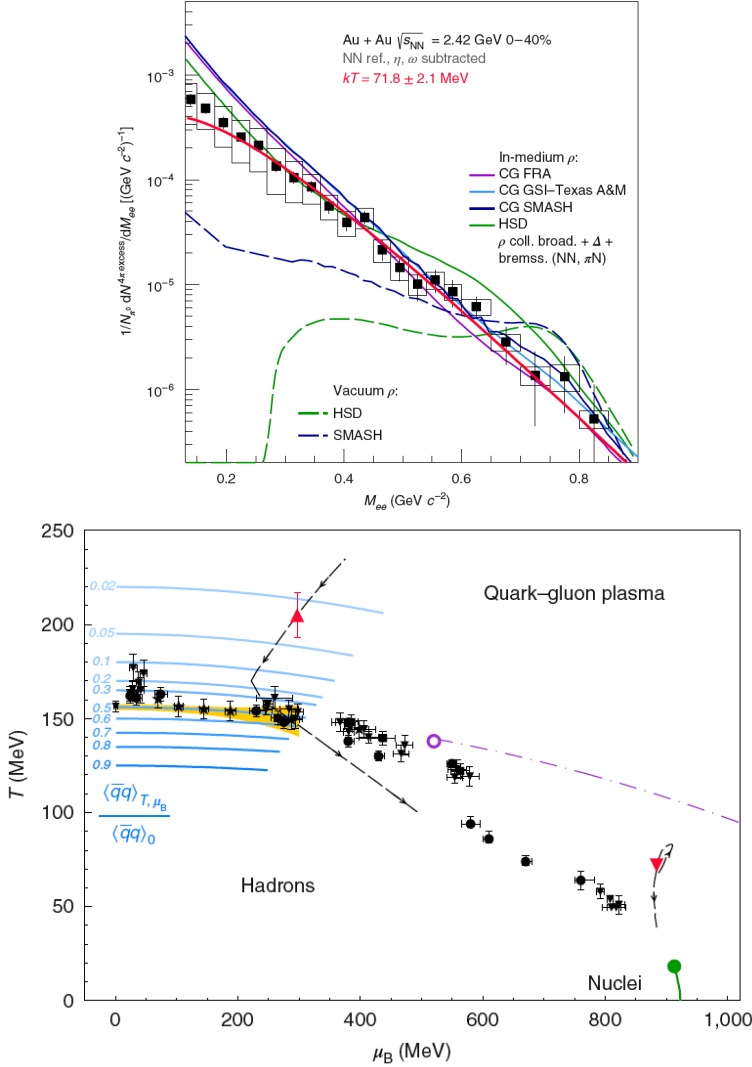


Fig. 17. Left: the acceptance corrected dielectron excess yield as a function of the dielectron mass M_{ee} as measured by HADES for the 0–40% most central Au+Au collisions at $\sqrt{s_{NN}} = 2.42$ GeV. The red curve corresponds to a fit with $dN/dM_{ee} \propto M_{ee}^{3/2} \exp(-M_{ee}/T)$. Right: the QCD phase diagram including chemical freeze-out points (black symbols) and early-stage temperatures as extracted by HADES and NA60 from intermediate-mass dilepton spectra (red symbols). Also shown are expectation values for the chiral condensate (blue lines), the crossover phase boundary as calculated with lattice-QCD (yellow band), and the conjectured trajectories of the reaction systems (black dashed lines) [8].

atically gather high-precision data, including very rare probes which up to now were inaccessible to experiments in this energy region. With this data new perspectives on the properties of the QCD phase diagram at high μ_B will open up, such as potential evidence for a first-order phase boundary or, ultimately, the location of a possible critical endpoint.

REFERENCES

- [1] F. Gao, J.M. Pawłowski, «Chiral phase structure and critical end point in QCD», *Phys. Lett. B* **820**, 136584 (2021).
- [2] BRAHMS Collaboration (I.G. Bearden *et al.*), «Nuclear Stopping in Au+Au Collisions at $\sqrt{s_{NN}} = 200$ GeV», *Phys. Rev. Lett.* **93**, 102301 (2004).
- [3] NA49 Collaboration (C. Blume), «Centrality and energy dependence of proton, light fragment and hyperon production», *J. Phys. G: Nucl. Part. Phys.* **34**, S951 (2007).
- [4] C. Blume, C. Markert, «Strange hadron production in heavy ion collisions from SPS to RHIC», *Prog. Part. Nucl. Phys.* **66**, 834 (2011).
- [5] A. Andronic, P. Braun-Munzinger, J. Stachel, «Thermal hadron production in relativistic nuclear collisions: The hadron mass spectrum, the horn, and the QCD phase transition», *Phys. Lett. B* **673**, 142 (2009); *Erratum ibid.* **678**, 516 (2009).
- [6] LIGO Scientific, Virgo collaborations (B.P. Abbott *et al.*), «GW170817: Observation of Gravitational Waves from a Binary Neutron Star Inspiral», *Phys. Rev. Lett.* **119**, 161101 (2017).
- [7] L. Tolos, «Dense Hadronic Matter in Neutron Stars», *Acta Phys. Pol. B* **55**, 5-A1 (2024), this issue, [arXiv:2401.09925 \[nucl-th\]](https://arxiv.org/abs/2401.09925).
- [8] HADES Collaboration (J. Adamczewski-Musch *et al.*), «Probing dense baryon-rich matter with virtual photons», *Nat. Phys.* **15**, 1040 (2019).
- [9] T. Galatyuk, «Future facilities for high μ_B physics», *Nucl. Phys. A* **982**, 163 (2019). Figure taken from: https://github.com/tgalatyuk/interaction_rate_facilities
- [10] STAR Collaboration (L. Adamczyk *et al.*), «Bulk properties of the medium produced in relativistic heavy-ion collisions from the beam energy scan program», *Phys. Rev. C* **96**, 044904 (2017).
- [11] STAR Collaboration (J. Adam *et al.*), «Strange hadron production in Au+Au collisions at $\sqrt{s_{NN}} = 7.7, 11.5, 19.6, 27, \text{ and } 39$ GeV», *Phys. Rev. C* **102**, 034909 (2020).
- [12] STAR Collaboration (M.S. Abdallah *et al.*), «Measurements of Proton High Order Cumulants in $\sqrt{s_{NN}} = 3$ GeV Au+Au Collisions and Implications for the QCD Critical Point», *Phys. Rev. Lett.* **128**, 202303 (2022).
- [13] STAR Collaboration (M.S. Abdallah *et al.*), «Disappearance of partonic collectivity in $\sqrt{s_{NN}} = 3$ GeV Au+Au collisions at RHIC», *Phys. Lett. B* **827**, 137003 (2022).

- [14] H.P. Zbroszczyk, «Results from the BES Program at RHIC», *Acta Phys. Pol. B Proc. Suppl.* **16**, 1-A18 (2023).
- [15] HADES Collaboration (G. Agakishiev *et al.*), «Statistical hadronization model analysis of hadron yields in p+Nb and Ar+KCl at SIS18 energies», *Eur. Phys. J. A* **52**, 178 (2016).
- [16] V. Friese, «Exploring Dense QCD Matter With the CBM Experiment», presented at the LXIII Cracow School of Theoretical Physics *Nuclear Matter at Extreme Densities and High Temperatures*, Zakopane, Poland, 17–23 September, 2023.
- [17] CBM Collaboration (T. Abyazimov *et al.*), «Challenges in QCD matter physics — The scientific programme of the Compressed Baryonic Matter experiment at FAIR», *Eur. Phys. J. A* **53**, 60 (2017).
- [18] A. László, «Recent results from the NA61/SHINE experiment on the critical point and onset of deconfinement», presentation at the Workshop on Critical Point and Onset of Deconfinement (CPOD 2022), 28 November–2 December, 2022.
- [19] E. Scomparin, «Quo Vadis NA60++», presentation at the Workshop on Critical Point and Onset of Deconfinement (CPOD 2022), 28 November–2 December, 2022.
- [20] A. Rustamov, «Deciphering Phase Transitions via Event-by-Event Particle Number Fluctuations and Correlation», presented at the LXIII Cracow School of Theoretical Physics *Nuclear Matter at Extreme Densities and High Temperatures*, Zakopane, Poland, 17–23 September, 2023, (pdf).
- [21] W. Reisdorf, H.G. Ritter, «Collective Flow in Heavy-ion Collisions», *Annu. Rev. Nucl. Part. Sci.* **47**, 663 (1997).
- [22] N. Herrmann, J.P. Wessels, T. Wienold, «Collective Flow in Heavy-ion Collisions», *Annu. Rev. Nucl. Part. Sci.* **49**, 581 (1999).
- [23] H.G. Ritter, R. Stock, «Collective flow of QCD matter: a historical introduction», *J. Phys. G: Nucl. Part. Phys.* **41**, 124002 (2014).
- [24] U. Heinz, R. Snellings, «Collective flow and viscosity in relativistic heavy-ion collisions», *Annu. Rev. Nucl. Part. Sci.* **63**, 123 (2013).
- [25] E. Schnedermann, J. Sollfrank, U.W. Heinz, «Thermal phenomenology of hadrons from 200A GeV S+S collisions», *Phys. Rev. C* **48**, 2462 (1993).
- [26] HADES Collaboration (J. Adamczewski-Musch *et al.*), «Directed, Elliptic, and Higher Order Flow Harmonics of Protons, Deuterons, and Tritons in Au+Au Collisions at $\sqrt{s_{NN}} = 2.4$ GeV», *Phys. Rev. Lett.* **125**, 262301 (2020).
- [27] HADES Collaboration (J. Adamczewski-Musch *et al.*), «Proton, deuteron and triton flow measurements in Au+Au collisions at $\sqrt{s_{NN}} = 2.4$ GeV», *Eur. Phys. J. A* **59**, 80 (2023).
- [28] S. Huth *et al.*, «Constraining Neutron-Star Matter with Microscopic and Macroscopic Collisions», *Nature* **606**, 276 (2022).

- [29] F. Becattini, M.A. Lisa, «Polarization and Vorticity in the Quark–Gluon Plasma», *Annu. Rev. Nucl. Part. Sci.* **70**, 395 (2020).
- [30] Z.-T. Liang, X.-N. Wang, «Globally Polarized Quark–Gluon Plasma in Noncentral A+A Collisions», *Phys. Rev. Lett.* **94**, 102301 (2005); *Erratum ibid.* **96**, 039901 (2006).
- [31] Y.B. Ivanov, «Global Λ polarization in moderately relativistic nuclear collisions», *Phys. Rev. C* **103**, L031903 (2021).
- [32] HADES Collaboration (R. Abou Yassine *et al.*), «Measurement of global polarization of Λ hyperons in few-GeV heavy-ion collisions», *Phys. Lett. B* **835**, 137506 (2022).
- [33] Y. Guo *et al.*, «Hyperon polarization from the vortical fluid in low-energy nuclear collisions», *Phys. Rev. C* **104**, L041902 (2021).
- [34] NA49 Collaboration (C. Alt *et al.*), «Pion and kaon production in central Pb+Pb collisions at 20A and 30A GeV: Evidence for the onset of deconfinement», *Phys. Rev. C* **77**, 024903 (2008).
- [35] A. Andronic, P. Braun-Munzinger, J. Stachel, H. Stocker, «Production of light nuclei, hypernuclei and their antiparticles in relativistic nuclear collisions», *Phys. Lett. B* **697**, 203 (2011).
- [36] S. Gläsel *et al.*, «Cluster and hypercluster production in relativistic heavy-ion collisions within the parton–hadron-quantum-molecular-dynamics approach», *Phys. Rev. C* **105**, 014908 (2022).
- [37] STAR Collaboration (J. Adam *et al.*), «Measurement of the mass difference and the binding energy of the hypertriton and antihypertriton», *Nat. Phys.* **16**, 409 (2020).
- [38] S. Spies, «HADES Overview», presentation at the 30th Conference on Ultra-Relativistic Nucleus–Nucleus Collisions (Quark Matter 2023), Houston, USA, 3–9 September, 2023.
- [39] ALICE Collaboration (S. Acharya *et al.*), « ${}^3_4\text{H}$ and ${}^3_4\bar{\text{H}}$ lifetime measurement in Pb–Pb collisions at $\sqrt{s_{\text{NN}}} = 5.02$ TeV via two-body decay», *Phys. Lett. B* **797**, 134905 (2019).
- [40] NA60 Collaboration (H.J. Specht), «Thermal Dileptons from Hot and Dense Strongly Interacting Matter», *AIP Conf. Proc.* **1322**, 1 (2010).